Prefibrillar Aggregates

DOI: 10.1002/anie.201003373

Characterizing Early Aggregates Formed by an Amyloidogenic Peptide by Mass Spectrometry**

Harriet L. Cole, Jason M. D. Kalapothakis, Guy Bennett, Perdita E. Barran, and Cait E. MacPhee**

Self-assembly of peptides and proteins into the ordered fibrillar aggregates known as amyloid fibrils has potential for achieving control over molecular-level architecture and macroscopic properties. Polypeptide fibrils have been suggested as templates for ordering inorganic components in nanoassemblies,[1] or as the basis for biomaterials.[2–4] The ordered self-assembly of proteins and polypeptides is also of interest in the context of the protein misfolding disorders, including Alzheimer's disease and type 2 diabetes. The vast majority of systems that form amyloid-like fibrils assemble by a nucleation and growth mechanism[5] whereby the formation of a multimeric nucleus of polypeptide molecules drives self-assembly. The considerable experimental difficulties associated with observing a small and potentially rare aggregate or aggregates in a soup of molecules have impeded characterization of these triggers to growth.

Herein we probe by time-course mass spectrometry (MS) and ion-mobility mass spectrometry (IM-MS) the early aggregation states of an amyloidogenic endecapeptide (sequence YTIAALLSPYS) derived from amino acid residues 105–115 of the human plasma protein transthyretin (TTR 105–115). The mobility K of an ion (and its corresponding reduced mobility K_0) is obtained from the arrival-time distribution (ATD) of a given ion after it has passed through a drift cell filled with a buffer gas under the influence of a weak electric field. K is inversely related to the orientationally averaged collision cross-section Ω by a modified version of Equation (1):

$$K_0 = \frac{3ze}{16N_0}\left(\frac{2\pi}{\mu k_B T}\right)^{1/2}\frac{1}{\Omega} \quad (1)$$

where z is ion charge, e is electron charge, N_0 the buffer gas number density, μ the reduced mass of the buffer gas and ion, k_B the Boltzmann constant, T the effective temperature, and Ω is the momentum transfer collision integral.

[*] Dr. J. M. D. Kalapothakis, G. Bennett, Dr. P. E. Barran
School of Chemistry, University of Edinburgh
Joseph Black Building, West Mains Road, Edinburgh EH9 3JJ (UK)
E-mail: perdita.barran@ed.ac.uk
H. L. Cole, Dr. C. E. MacPhee
SUPA, School of Physics and Astronomy, University of Edinburgh
JCMB, Mayfield Road, Edinburgh EH9 3JZ (UK)
E-mail: cait.macphee@ed.ac.uk

[**] This research was funded by the EPSRC, the BBSRC, and the British Mass Spectrometry Society. C.E.M. is a Royal Society University Research Fellow.

Supporting information for this article is available on the WWW under http://dx.doi.org/10.1002/anie.201003373.

The use of MS methods, and in particular IM-MS, can provide molecular detail on the early stages of aggregation of amyloidogenic peptides and proteins. A large body of work assessing the configurations of species formed during polypeptide aggregation has utilized MS techniques: for example, Bowers and co-workers have examined the self-assembly of Aβ,[6] α-synuclein,[7] IAPP,[8] and most recently a prion protein fragment.[9] The unique benefit of this approach is illustrated by a study of early aggregate species formed by the Alzheimer's-related peptide Aβ1-42 and the non-amyloidogenic variant Aβ1-42 F19P (by Bernstein and co-workers[10]). Resolved species in an ATD following nESI–MS of Aβ1-42 were assigned to dimer, tetramer, hexamer, and dodecamer ($n = 1$, 2, 3, and 6 respectively) whereas the F19P mutant contained only dimer and tetramer. Furthermore, the absence of aggregates intermediate between putative hexamers and dodecamers led the authors to speculate that the hexamer was the building block of protofibril formation, a finding corroborated by cross-linking studies.[11–13] Recent work by Ashcroft and co-workers[14] describes the conformation of β2m oligomers up to the tetramer, finding compact dimers and elongated trimers and tetramers. These studies and others demonstrate that IM-MS (often combined with simulations) provides useful insight into the events that occur during the early stages of fibril aggregation, including delineating the structure of the monomer, identifying oligomer distributions, and revealing mechanistic details of the aggregation process. Herein we extend current approaches by using IM-MS to examine the change in the population of oligomers present in solution over an eight-hour time period. We present the distribution of oligomers identified using nano-electrospray ionization (nESI) mass spectrometry and their collision cross-sections (CCS), and compare the change in the population of oligomers and in their CCSs as a function of time. Experimental CCSs are compared with those obtained by molecular mechanics modeling.

Figure 1 is a typical nESI mass spectrum obtained from a solution of the TTR 105–115 peptide immediately after resuspension. Oligomers of the general form $[nM + z\,\mathrm{H}]^{z+}$ are observed with $1 \le n \le 13$. With the notable exceptions of the work of Ashcroft et al. on β2m[15] and that of Nettleton et al. on bovine insulin,[16] our observation of a wide range of oligomers is atypical of amyloidogenic systems. The spectrum is dominated by a peak at m/z 1202.0, corresponding to both $[M{+}\mathrm{H}]^+$ and $[2M{+}2\,\mathrm{H}]^{2+}$, with other high-abundant ions at m/z 601.5, 1502.4, 1601.8, and 1441.8 assigned to $[M{+}2\,\mathrm{H}]^{2+}$, $[5M{+}4\,\mathrm{H}]^{4+}$, $[4M{+}3\,\mathrm{H}]^{3+}$, and $[6M{+}5\,\mathrm{H}]^{5+}$, respectively. Each oligomer is found in relatively few protonation states, which is similar to the findings of Bowers et al. for Aβ.[17] With the sole

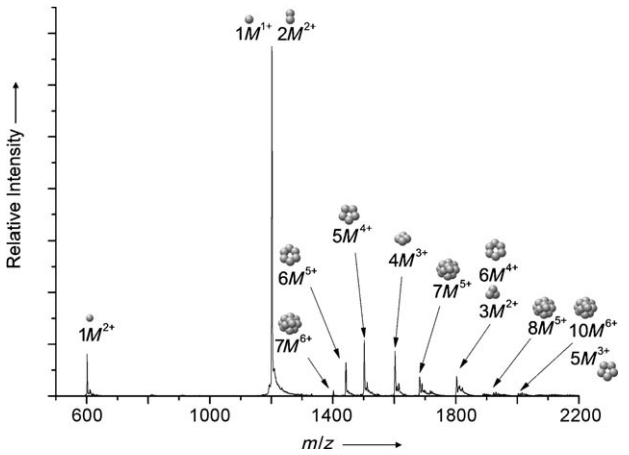

Figure 1. An annotated n-ESI mass spectrum showing the TTR (105–115) oligomers present and their associated charge states. Under non-aggregating conditions the peptide is observed predominantly as a monomer with a small contribution from dimer; no higher-order aggregates are observed. Pictured oligomers are for illustrative purposes only and do not correspond to validated structures.

exception of the doubly-charged monomer, all of the observed species carry fewer charges than the number of peptides in the oligomer. This finding suggests that the ions adopt compact geometries, as a large number of charges will increase the CCS of an aggregate owing to Coulombic repulsion;[18,19] IM-MS analysis (see below) quantifies this point.

Figure 2 shows the relative intensities of all of the species detected at $t=0$ shown as a function of multimeric order. Species present were assigned using spacings owing to the presence of potassium adducts within a given peak envelope, combined with ATD data (see below).

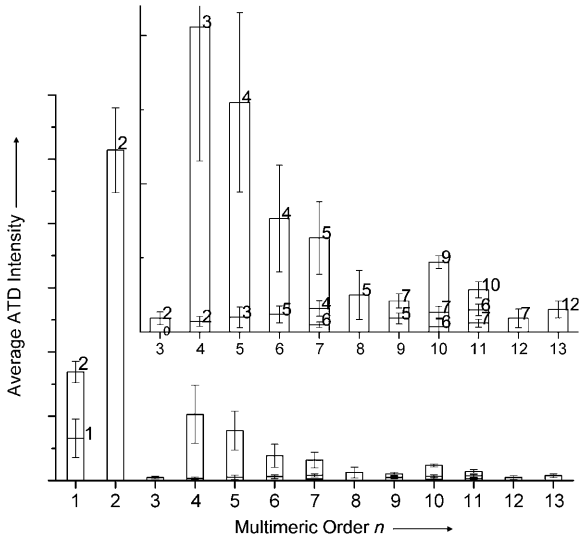

Figure 2. Distribution of oligomers at $t=0$: Each bar represents the maximum intensity of the ATD for each oligomer at a drift voltage of 50 V. Where more than one charge state is observed, the bar is divided proportionately. Charge states are indicated by the number above the bar. The inset shows an expansion of the region for $n>2$. The data are averaged over three repeats; error bars represent the standard deviation.

When the data are viewed in this way, it is obvious that some species are dominant. The peak at 1202.0 corresponds mainly to $[2M+2\,H]^{2+}$, thus the dimer is the most abundant species. The tetramer and pentamer are also seen in high abundance, the former solely as the ion $[4M+3\,H]^{3+}$ and the latter principally as the ion $[5M+4\,H]^{4+}$. Where more than one charge state is observed, one value of z typically dominates. A very weak signal from the trimer is visible, which points to an instability for this species relative to the dimer and tetramer. Contributions from other oligomers decay exponentially, with the exception of the $[10M+z\,H]^{z+}$, which appears as a stable magic-number oligomer.[20] Figure 2 also shows that the higher-order aggregates are observed in unequal charge states: for example $[10M+z\,H]^{z+}$ is seen with $z=6$, 7, and 9 but not 8; $[9M+z\,H]^{z+}$ is observed with $z=5$ and 7 but not 6; and $[11M+z\,H]^{z+}$ is present as $z=6$, 7, and 10 but not 8 and 9. Charge states that are not observed may be too weak to be detected, and for some, m/z values are coincident with very abundant species of lower oligomeric order; nonetheless they appear to have a lower stability that may be due to the adoption of favorable conformations by only some oligomers. We speculate that this is due to anti-parallel or parallel arrangements of polypeptide chains that favor only certain charge and aggregation states.

Using the ion-mobility capabilities of our instrument,[21] CCSs were determined for all of the species shown in Figure 1 and 2. Results from this analysis are shown in Figure 3 and tabulated in the Supporting Information, Table S1. As expected, an increase in CCS with oligomer order is observed. Variation from a monotonic rate of increase in CCS with oligomer number reveals interesting features from which structural information can be inferred.

Oligomer CCSs increase in a linear fashion for the highest charge state for each oligomer, which is to be expected, but what is more interesting is the lack of increase in CCS as a function of n when $n>3$. For example, the CCSs for $n=4$ and

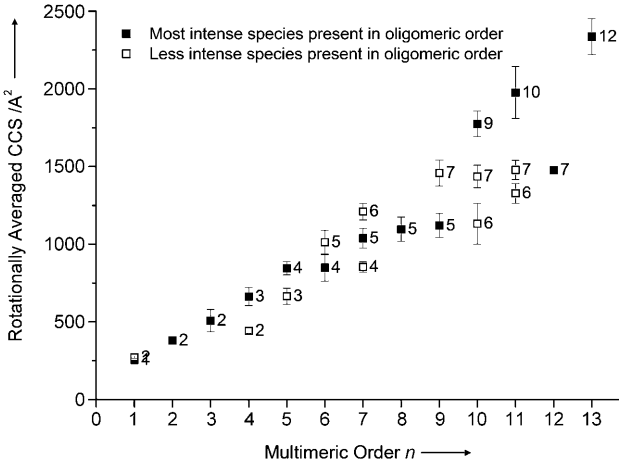

Figure 3. CCS at $t=0$: Graph showing the collision cross-sections of all species observed at $t=0$. The data are averaged over 5 repeats; error bars reflect the standard deviation of the mean. For each oligomer the most intense charge state is indicated. For oligomers above $n=9$ the difference in abundance between charge states is small.

5 are very similar when $z = 3$ (Figure 3), and the CCSs of the hexamer, heptamer, octamer, and nonamer are within 10% when $z = 5$ despite an increase in mass of $> 60\%$. Where an oligomer is present in a range of charge states, the CCSs do increase with charge. Thus packing to form a dense aggregate competes with Coulombic repulsion to determine the final CCS of the oligomer.

Within any oligomer, the amino group at the N terminus of each peptide is available for protonation. It is also possible that the proline residue is protonated, which may account for the observed $[M+2H]^{2+}$ species, although this is less likely. If this protonated group is packed in the interior of the aggregate and therefore inaccessible, the oligomer will carry a low net charge relative to the number of peptides; if it is surface-exposed, ionization will drive charge–charge repulsion, Coulombic destabilization, and expansion of the aggregate. Our observation that all of the species carry fewer charges than the number of peptides in the oligomer, as well as the comparatively small increase in CCS with a large increase in mass, suggest dense packing. Moreover, given the sequence of TTR 105–115 it is likely that this packing is governed by hydrophobic interactions; as these are weakened in the gas phase, we argue that the species we detect must have been preserved intact from solution into the gas phase.

Given atomic co-ordinates, it is possible to calculate a CCS that can be compared to one measured by experiment.[19,22,23] Using the AMBER force field, likely candidate geometries for TTR 105–115 oligomers were modeled using a simulated annealing approach. We consider the lowest energy structures as likely candidates for comparison with experimental measurements. For all oligomers, we observed the formation of collapsed globular structures (Supporting Information, Figure S2). Experimentally observed CCSs are consistently smaller than the calculated structures (Table 1). Moreover, experimental cross-sections increase with oligomeric order at a rate lower than those of the calculated structures.

Experimental factors may contribute to such a discrepancy; for example, the presence of unresolved higher-order oligomeric ions under the ATDs analyzed might contribute to a lower CCS. Another contribution to this could be the presence of a protonated proline, a form not considered in our calculations. That being said, comparison between simulation and experiment is consistent with the adoption of condensed structures, and suggests that the solution-phase structures are even more densely packed than those observed by simulation.

Table 1: Comparison between theoretically calculated and experimental collision cross-sections.

Ionic species	Collision cross-sections [Å^2]	
	calculation[a]	experiment
$[M+H]^+$	270.0	256 ± 6
$[2M+H]^+$	441.1	380 ± 13[b]
$[3M+2H]^{2+}$	567.0	509 ± 36
$[4M+3H]^{3+}$	737.0	663 ± 28
$[5M+4H]^{4+}$	878.0	847 ± 22

[a] Values are taken from an average of all of the 300 calculated structures, with a Boltzmann weighting on their energy. [b] Experimental data not available for $[2M+H]^+$; data is CCS of $[2M+2H]^{2+}$.

Figure 4 shows mass spectra taken at intervals over an eight-hour period, which is within the lag phase of TTR 105–115 self-assembly.[24] For the first 4 h there is a rise in the observable oligomer population followed by a rapid decline in most of the aggregates, with the exception of the monomer, dimer (not shown in Figure 4a), and tetramer species, which persist over the period of study. When the dominant peak at 1202.0 is viewed in ATD space, the proportion attributable to dimer and monomer is seen to vary with time (Figure 4b). Initially there is far more $[2M+2H]^{2+}$ present than $[M+H]^+$; however, at 4 h this is no longer the case and we observe relative enrichment of the monomer. At both the 6 h and 8 h time points, the proportion of dimer is seen to rise again. The abundance of monomer at 4 h must originate from the break-up of unstable higher order aggregates owing to destabilization either in solution or upon desolvation. The data show a particular and significant persistence of dimer and tetramer

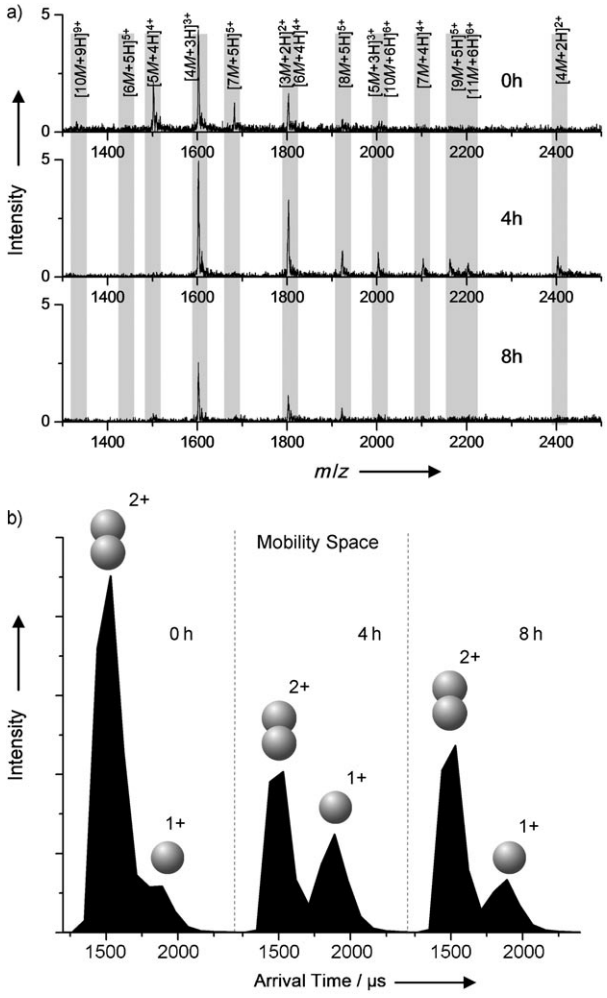

Figure 4. a) Time course spectra, created by scanning over the same number of scans at a drift voltage of 50 V. Spectra shown are representative of all data. Peaks are labeled to show their oligomeric order and charge assignations. b) Arrival time distributions for the species $[2M+2H]^{2+}$ and $[M+H]^+$ measured at 0 h, 4 h, and 8 h with a drift voltage of 50 V, averaged over 3 repeats. m/z for $[M+H]^+$ and $[2M+2H]^{2+}$ are coincident; however, these species are deconvoluted in mobility space by their arrival times.

whilst the other more transient oligomers contribute either to aggregation or off-pathway processes. The presence of the tetramer in an on-pathway process would be consistent with previous data, suggesting that the minimal unit of the mature fibril is assembled from four β-sheets in a "cross-β" configuration.[24] Plotting the CCS as a function of time demonstrates a systematic increase in CCS for the majority of oligomers with $n > 4$ (Supporting Information, Figure S1), whilst the CCSs remain constant for the smaller oligomers. This observation is consistent with dynamic rearrangement of the larger $n > 4$ oligomers and the adoption of increasingly extended, possibly β-strand-like, conformations.

This work shows that ion-mobility mass spectrometry provides a detailed insight into the molecular associations that ultimately lead to amyloid-like fibril formation. The amyloidogenic TTR (105–115) peptide forms a large variety of aggregates during the early stages of fibrillogensis. We observe densely packed oligomers that are dominated by hydrophobic interactions, and dynamic remodeling of these oligomers during the lag phase prior to fibril assembly. It is not possible to assess which of the many species are responsible for on-pathway aggregation leading to the assembly of amyloid-like fibrils, however of particular note is our observation of a stable tetrameric species, which is consistent with the dimensions of the mature fibril. Also of note is our detection of a stable, compact, and unusually prevalent decamer. It is commonly accepted that oligomers formed early in the aggregation process are toxic to a wide variety of cell types and that disease may result from these "toxic oligomers"; we speculate that the transiently stable, compact, and prevalent decamer is a candidate for such a species.

Experimental Section

Ion-mobility mass spectrometry measurements were performed on an in-house modified QToF1 instrument (Micromass UK Ltd).[21] Further experimental details can be found in the Supporting Information (Methodology and Simulation Strategies).

Received: June 3, 2010
Published online: October 28, 2010

Keywords: amyloids · ion mobility · mass spectrometry · oligomers · polypeptides

[1] A. J. Baldwin, R. Bader, J. Christodoulou, C. E. MacPhee, C. M. Dobson, P. D. Barker, *J. Am. Chem. Soc.* **2006**, *128*, 2162–2163.
[2] H. Kodama, S. Matsumura, T. Yamashita, H. Mihara, *Chem. Commun.* **2004**, 2876–2877.
[3] C. E. MacPhee, C. M. Dobson, *J. Am. Chem. Soc.* **2000**, *122*, 12707–12713.
[4] K. Channon, C. E. MacPhee, *Soft Matter* **2008**, *4*, 647–652.
[5] T. R. Serio, A. G. Cashikar, A. S. Kowal, G. J. Sawicki, J. J. Moslehi, L. Serpell, M. F. Arnsdorf, S. L. Lindquist, *Science* **2000**, *289*, 1317–1321.
[6] D. B. Teplow, N. D. Lazo, G. Bitan, S. Bernstein, T. Wyttenbach, M. T. Bowers, A. Baumketner, J. E. Shea, B. Urbanc, L. Cruz, J. Borreguero, H. E. Stanley, *Acc. Chem. Res.* **2006**, *39*, 635–645.
[7] S. L. Bernstein, D. F. Liu, T. Wyttenbach, M. T. Bowers, J. C. Lee, H. B. Gray, J. R. Winkler, *J. Am. Soc. Mass Spectrom.* **2004**, *15*, 1435–1443.
[8] M. E. Sardiu, Y. Cai, J. Jin, S. K. Swanson, R. C. Conaway, J. W. Conaway, L. Florens, M. P. Washburn, *Proc. Natl. Acad. Sci. USA* **2008**, *105*, 1454–1459.
[9] M. Grabenauer, C. Wu, P. Soto, J.-E. Shea, M. T. Bowers, *J. Am. Chem. Soc.* **2010**, *132*, 532–539.
[10] S. L. Bernstein, T. Wyttenbach, A. Baumketner, J. E. Shea, G. Bitan, D. B. Teplow, M. T. Bowers, *J. Am. Chem. Soc.* **2005**, *127*, 2075–2084.
[11] H. Levine, *Neurobiol. Aging* **1995**, *16*, 755–764.
[12] G. Bitan, A. Lomakin, D. B. Teplow, *J. Biol. Chem.* **2001**, *276*, 35176–35184.
[13] G. Bitan, M. D. Kirkitadze, A. Lomakin, S. S. Vollers, G. B. Benedek, D. B. Teplow, *Proc. Natl. Acad. Sci. USA* **2003**, *100*, 330–335.
[14] D. P. Smith, S. E. Radford, A. E. Ashcroft, *Proc. Natl. Acad. Sci. USA* **2010**, *107*, 6794–6798.
[15] A. M. Smith, T. R. Jahn, A. E. Ashcroft, S. E. Radford, *J. Mol. Biol.* **2006**, *364*, 9–19.
[16] E. J. Nettleton, P. Tito, M. Sunde, M. Bouchard, C. M. Dobson, C. V. Robinson, *Biophys. J.* **2000**, *79*, 1053–1065.
[17] S. L. Bernstein, N. F. Dupuis, N. D. Lazo, T. Wyttenbach, M. M. Condron, G. Bitan, D. B. Teplow, J. E. Shea, B. T. Ruotolo, C. V. Robinson, M. T. Bowers, *Nat. Chem.* **2009**, *1*, 326–331.
[18] D. E. Clemmer, M. F. Jarrold, *J. Mass Spectrom.* **1997**, *32*, 577–592.
[19] M. F. Jarrold, *Annu. Rev. Phys. Chem.* **2000**, *51*, 179–207.
[20] Y. Yamada, A. W. Castleman, *J. Chem. Phys.* **1992**, *97*, 4543–4548.
[21] B. J. McCullough, J. Kalapothakis, H. Eastwood, P. Kemper, D. MacMillan, K. Taylor, J. Dorin, P. E. Barran, *Anal. Chem.* **2008**, *80*, 6336–6344.
[22] A. A. Shvartsburg, M. F. Jarrold, *Chem. Phys. Lett.* **1996**, *261*, 86–91.
[23] M. F. Mesleh, J. M. Hunter, A. A. Shvartsburg, G. C. Schatz, M. F. Jarrold, *J. Phys. Chem.* **1996**, *100*, 16082–16086.
[24] C. P. Jaroniec, C. E. MacPhee, V. S. Bajaj, M. T. McMahon, C. M. Dobson, R. G. Griffin, *Proc Natl. Acad. Sci. USA* **2004**, *101*, 711–716.

